Electronic Supplementary Material (ESI) for ChemComm.

Self-assembly and redox induced phase transfer of gold nanoparticles at the water-propylene carbonate interface

Evgeny Smirnov,[1] *Pekka Peljo,*[1] *and Hubert H. Girault*[1,*]

[1] Laboratoire d'Electrochimie Physique et Analytique, Ecole Polytechnique Fédérale de Lausanne, Rue de l'Industrie 17, CH-1951 Sion, Switzerland.

Table of Contents

SI-1. Experimental section

Chemicals

Tetrachloroauric acid (HAuCl4, 99.9%), tetrathiafulvalene (TTF) and propylene carbonate (PC) were received from Aldrich. Citrate trisodium dihydrate ($Na_3C_6H_5O_7 \cdot 2H_2O$) were purchased from Fluka. Silver nitrate ($AgNO_3$) was bought from Chempur and ascorbic acid ($C_6H_8O_6$) from Riedel-de-Haen. 1-hexadecanethiol was purchased from Alfa Aesar, and carboxy-terminated PEG thiol ($HS\text{-}(CH_2CH_2\text{-}O)_n\text{-}COOH$, M = 2 kDa) was supplied by Nanocs. All chemicals were used as received without further purification. In all experiments Millipore water (18.2MΩ cm) was used.

Synthesis of AuNPs and their characterization

Suspensions of AuNPs with various mean diameters were prepared using the seed-mediated growth method.[1] Seed particles for that method were synthesized by commonly used Turkevich method.[2,3] Details on procedure are given in Ref.4.

The obtained colloidal solution of AuNPs were characterized by UV-Vis-nearIR spectroscopy using a standard Cary8453 (Agilent) spectrophotometer with a 10 mm quartz cell. Also, all other UV-Vis-near IR measurements were carried out with this equipment. Mean diameter and concentration of nanoparticles in the prepared solution were determined as described by Haiss *et al.*[5] and were equal to 32 nm and 3×10^8 particles/μL.

The UV-Vis-nearIR response from obtained gold nanofilm was recorded in extinction mode as depicted in Scheme S1. As seen from the presented scheme, extinction from double film was collected.

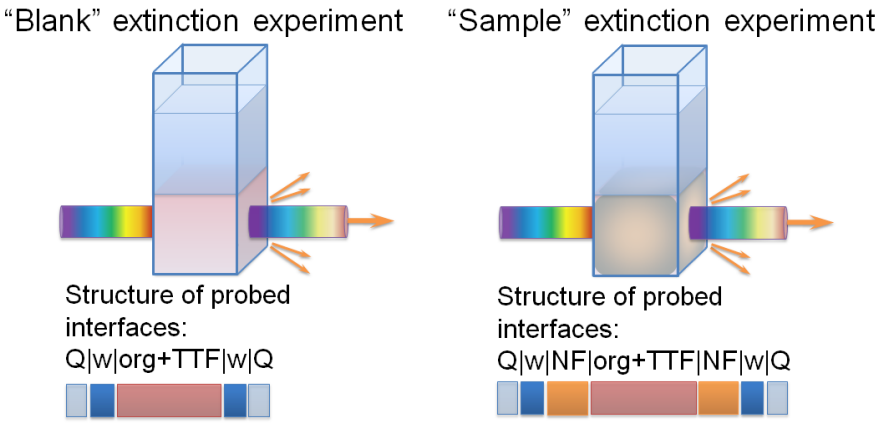

Scheme S1. Schematic representation of UV-Vis-nearIR measurement in extinction mode for a gold nanofilm.

Size and ζ-potential distributions was obtained by dynamic light scattering (DLS) measurements performed with a Nano ZS Zetasizer (Malvern Instruments, UK). For aqueous solution standard plastic cells were used, whereas AuNPs in PC phase were analysed in quartz cell equipped with ZEN1002 accessory.

Transmission electron microscopy (TEM) images were recorded using a Tecnai G2 Spirit Twin (FEI) high resolution transmission electron microscope (HR-TEM), operating

with a LaB_6 electron source at 120 kV. The size distributions of the AuNPs were estimated by using ImageJ software assuming that the AuNPs were spherical. For each sample 4 to 5 individual images were analysed, collecting information on more than 150 individual AuNPs.

Scanning TEM (STEM) images were obtained with FEI Titan Themis microscope equipped with high brightness X-FEG gun at 300kV and beam current of 0.5 nA. All images were acquired with HAADF detector. The mentioned microscope is equipped with 4 silicon drift Super-X detectors (Bruker, Germany) for EDX analysis and chemical mapping. Authors acknowledge Dr. Emad Oveisi for the help with that experiment at CIME facilities and fruitful discussion.

SI-2. Interfacial surface tension measurements by a pendant drop method

Pendant drop measurements were carried out on a drop shape analysis system DSA100 (Kruss, Germany). All glassware used was cleaned with a mixture of nitric and hydrochloric acid (*aqua regia*), washed several times with pure water, dried and then treated with oxygen plasma for 30 minutes in order to eliminate any presence of other compounds. Each organic solution was vigorously shaken with Milli-Q water and subsequently the biphasic system was left overnight in order to obtain saturated solutions (aqueous with organic phase and organic with aqueous phase, respectively).

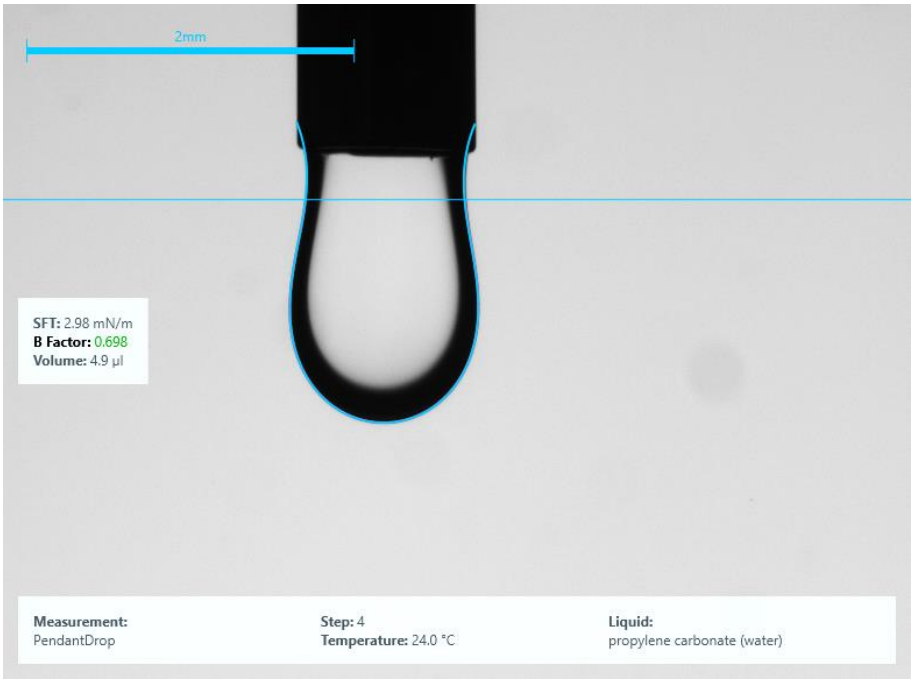

Figure S2. Pendant drop measurements of the interfacial surface tension($\gamma_{w/o}$) for water-PC biphasic system.

Based on shapes of the obtained pendant drops and physical properties of the solvent, the value for the interfacial tension was calculated as follows: γ(w-PC) = 2.95±0.05 mN·m^{-1}.

SI-3. STEM images and chemical mapping of TTF@AuNPs

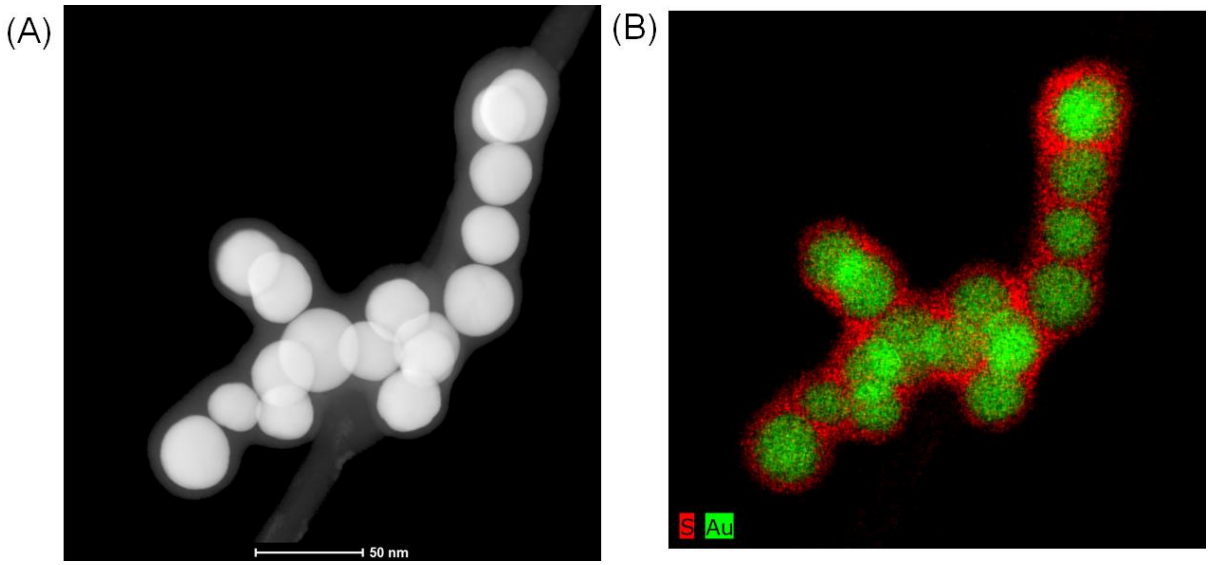

Figure S3. (A) STEM-image of TTF@AuNPs. (B) Chemical (EDX) mapping of the same sample showing presence of sulphur (TTF/$TTF^{+\bullet}$) layer on the surface of gold nanoparticles.

SI-4. Thermodynamic modelling of AuNP interaction with LLI

Theoretical description of the model used

According to Flatte's model,[6] the overall interaction potential consists of 4 main components: energy of capillary forces (W_{cap}), solvation energy (W_{solv}) or energy devoted to image-forces,[7] energy by external electric field (W_{ext}), and energy of line tension (W_{line}). The last one should include also any other kinds of relatively small interaction that push charged nanoparticles away from the interface. Thus, the cumulative energy (W_{sum}) is the sum of all mentioned items:

$$W_{sum} = W_{cap} + W_{solv} + W_{ext} + W_{line}$$

We worked with non-polarized interface, so $W_{ext} \equiv 0$.

For the potential description was as following:

$$W_{cap} = -\pi r^2 \gamma_{o/w} \left(\frac{4\cos(\theta)}{1+e^{-2x/r}} + \mathrm{e}^{-x^2/r^2} \right)$$

$$W_{solv} = k_B T \frac{Z^2}{2} \frac{L_B}{r} \left(\frac{\varepsilon_w}{\varepsilon_{oil}} \frac{1}{1+\kappa_{oil} r} - \frac{1}{1+\kappa_w r} \right) \frac{1}{1+e^{-x/r}}$$

$$W_{line} = 2\pi r \mu \, \mathrm{e}^{-x^2/2r^2}$$

where x is a coordinate, r is a nanoparticle radius, $\gamma_{o/w}$ is interfacial surface tension, θ is three phase contact angle, Z is a charge of nanoparticle, κ_{oil} and κ_w are Debye length for oil and water phases respectively, ε_{oil} and ε_w are dielectric constants for oil and water phases and L_B is length determined as $L_B = \frac{{q_e}^2}{4\pi\varepsilon_w\varepsilon_0 k_B T}$ (q_e is an elementary charge).

The calculation was carried out in *Mathematica*. The front-end program is available upon request to the corresponding author e-mail.

In the case of W_{line}, the assumption was made that the linear tension changes proportional to $\frac{\gamma_{w/PC}}{\gamma_{w/DCE}}$.

As mentioned in the main text, interaction of AuNPs with TTFs leads to: **(i)** reducing the positively charged core of NP by transfer of electrons from TTF and **(ii)** changing the wettability due to replacement citrate with more hydrophobic TTF.[8,9]

Assumptions about the net charge and wettability of a AuNP

Firstly, we should estimate the excess of charge of a single NP and limit the possible range of reasonable charges per NP. In previously published works[9,10,11] we clearly demonstrated that citrate@AuNPs should have a positively charged gold core. According to simple geometrical estimations (see Section 5 in ESI), we could talk here

about Z-range limited by +1000 – +1200 e^- for a single AuNP of 32 nm in diameter before interaction with TTF and *ca.* –1000 e^- after interaction with TTF. For thermodynamic modelling we chose Z = +400 and Z = –700 before and after interaction with TTF, respectively (Section 5 in ESI).

Secondly, interaction with TTF changes wettability of gold nanoparticles. Assuming only partial substitution of citrate, three phase contact angle θ was reduced from 88 to 60 degrees. For instance, the three phase contact angle for 100 nm citrate@AuNPs was reported previously as 82º at water-*n*-decane interface.[12]

Observed changes in energetic profiles

Simulation results are shown in Figure S4. Both the capillary energy, devoted to the contribution of the interfacial tension, and the solvation energy influenced equally the whole energy profile (Figure S4). For the Z = +400 (in the absence of TTF), both DCE and PC had a potential well localized at the vicinity of the interface. In the case of DCE, the depth of this well was around 1500 k_BT, however, this well was separated by a potential barrier of *ca.* 1000 k_BT from the bulk (Figure S4A). The latter means no interaction of nanoparticles with the interface. Nevertheless, for the PC-water interface, the potential barrier was less than 100 k_BT, while the well was *ca.* 250 k_BT in depth (Figure S4B). Therefore, nanoparticles may overcome that barrier during shaking and emulsification, when formation of additional surfaces lowers the value of the barrier almost to zero and attachment of the particles to the LLI is favorable.

Reduction of AuNPs by TTF significantly decreased the potential barrier and increased the depth of the potential well in both cases DCE and PC. For DCE it led to a deeper potential well and stabilization of the whole system in the *nanofilm* state, gaining a couple of thousands k_BT by accumulating particles at the interface. This high potential barrier cannot be overcome only by emulsification, but rather by emulsification and a homogeneous reaction of TTF with AuNPs and the following formation of weakly bonded aggregates prior landing them at the LLI.[8] The energetic profile for the PC-water interface was dramatically different. The potential barrier on the aqueous side disappeared and AuNPs could easily slide into the oil phase.

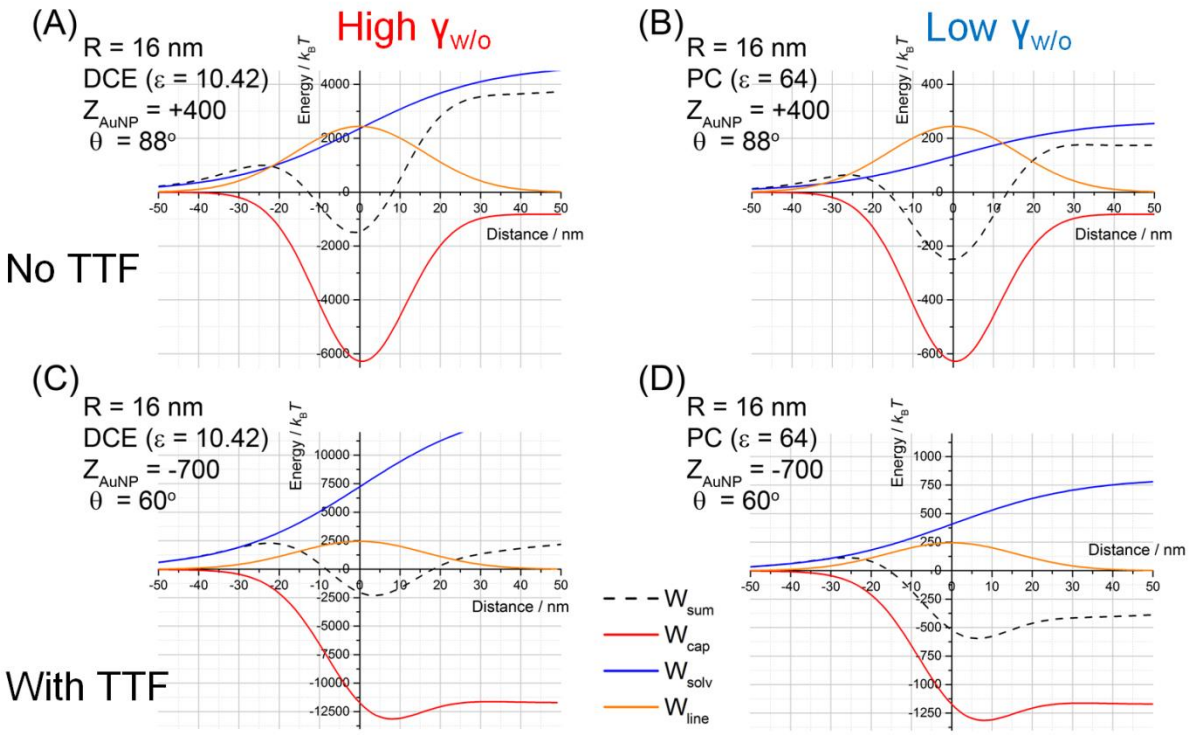

Figure S4. Contribution of components: capillary forces, solvation and line tension to overall energy profiles at LLIs. Energy profiles at liquid-liquid interfaces: **(A, C)** water-DCE and **(B, D)** water-PC are presented for the following parameter sets: **(A, B)** bare water-PC interface Z=+400, θ = 88º, R=16nm and **(C, D)** water-PC interface with presence of TTF Z=-700, θ = 60º, R=16nm.

Concerning the potential barrier

The potential barrier on the aqueous side exists all the time, as particles are charged. It blocks the interface from nanoparticles and prevents their landing at the interface to reduce entire excess of surface energy. The reason of that is the energetic profile of capillary (W_{cap}) and solvation forces (W_{solv}). Thus, for example, W_{cap} has $\frac{1}{1+e^{-2x/r}}$ dependence, whereas W_{solv} has $\frac{1}{1+e^{-x/r}}$, which extends further than W_{cap}.

There is only one way how W_{cap} can overtake W_{solv} – significantly reduced charge (or more generally, charge density) of nanoparticles. Thus, we come out to the classical Pickering emulsions, where relatively large particles with relative low surface charge are spontaneously self-assemble at LLI.

For instance, similar behavior could be achieved with AuNPs, if we assume neglected surface charge, below 10-20 unit charge per particle. In that case, the barrier almost disappears and only a potential well is left over.

However, in real situation we deal with small particles and relatively high surface charges, thus, the solvation energy is the main “enemy” for spontaneous self-assembly.

To the question of the driving force

The presented conclusions seem controversial to a common sense, which tell us that the higher surface tension, the higher energetic gain from adsorption of nanoparticles at s LLI. It is obvious that the higher surface tension the higher driving force. Nevertheless, if this driving force or gain in energy is protected (or "hidden" behind) the potential barrier, it cannot influence nanoparticles in the bulk. They simply do not feel any potential well behind the potential wall.

Of course, there is a pretty low probability that a NP in the bulk will get somehow enough energy to overcome the barrier and will be entrapped by the interface. For example, such events were observed as assembly of tiny golden islands at water-air interface while storing the solution of nanoparticles.

To conclude, on the one hand reduction in interfacial tension reduces the depth of the potential well and, therefore, the driving force. However, on the other hand, it diminishes the potential barrier, that separates the interfaces from the bulk with nanoparticles, and, thus, makes possible self-assembly of nanoparticles at the bare interface.

The interfacial transfer of AuNPs

The PC phase has higher dielectric constant (ε_{PC} = 64) than DCE (ε_{DCE} = 10) that significantly facilitates transfer of partially charged AuNPs to the oil phase in the presence of TTF or their assembly at the interface in the absence of TTF. However, as shown here, the role of the interfacial tension was crucial in this case, as only at low interfacial tensions nanoparticles are transfer through the interface (no potential well at the interface).

To conclude, the interplaying between surface tension and the nature of the solvent will mostly determine the interfacial process: self-assembly at a LLI or transfer across a LLI.

SI-5. Estimation of charge on a single gold nanoparticle

To estimate the excess of charge on a single spherical NP we used geometrical parameter for molecules such as citrate and TTF, refined in Chem3D (Cambridge Soft) with MM2 algorithm (Figure S4). Dimensions of TTF and citrate molecules were calculated as 0.8572 x 0.3092 nm and 0.6696 x 0.4493 nm, respectively. Correspondingly, surface areas (S_{mol}) are equal to 0.2650 and 0.3008 nm^2, respectively. However, taking into account electron clouds and Coulombic repulsion we should multiply these area values by 9 or 10 at least (lateral dimensions will be multiplied by 3), giving enough room to accommodate molecules and charge on the surface of AuNP. Thus, it results in 2.6 and 3 nm^2 per molecule.

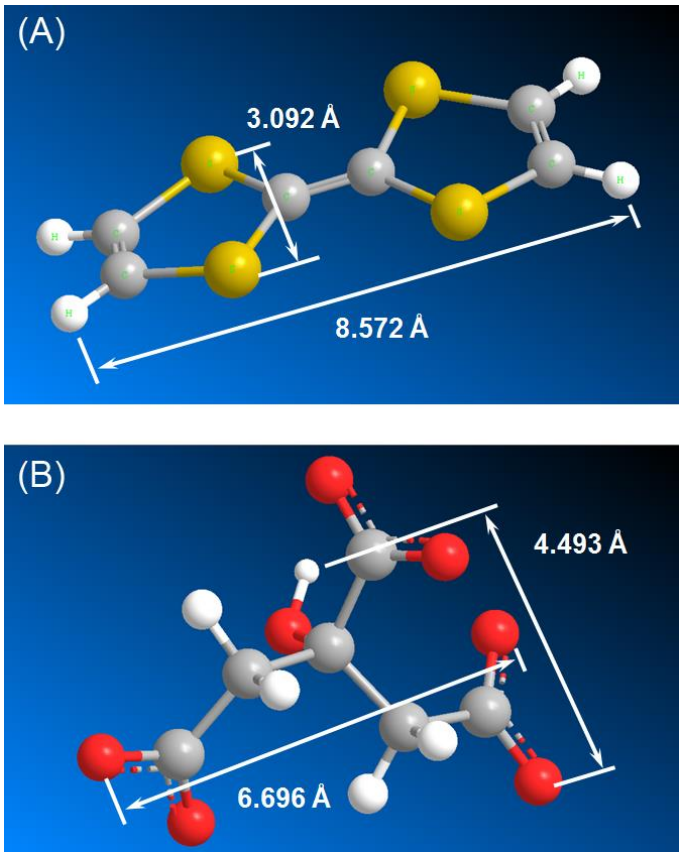

Fig.S5. Structures of TTF and citrate molecules drawn and refined in Chem3D software package with MM2 algorithm.

The surface area of a spherical NP of 16 nm in diameter is $S_{sphere} = 3217 nm^2$.

Amount of sorbet molecules is determined by the ratio S_{sphere} / S_{mol}, which gives around 1240 citrate and 1072 TTF molecules per a single nanoparticle of 16 nm in radius in the case of molecules close-packing. Thus, this estimation is the upper limit.

Therefore, the realistic values of Z (positive charge on AuNP's core) is about +400-500e^-, but do not exceed +1000-1200 e^-.

SI-6: Supplementary references:

1. Y.-K. Park, S.-H. Yoo, and S. Park, *Langmuir*, 2007, **23**, 10505–10.
2. J. Turkevich, P. C. Stevenson, and J. Hillie, *Discuss. Faraday Soc.*, 1951, **11**, 75–82.
3. G. Frens, *Nat. Phys. Sci.*, 1973, **241**, 20.
4. E. Smirnov, P. Peljo, M. D. Scanlon, F. Gumy, and H. H. Girault, *Nanoscale*, 2016, **8**, 7723–7737.
5. W. Haiss, N. T. K. Thanh, J. Aveyard, and D. G. Fernig, *Anal. Chem.*, 2007, **79**, 4215–21.
6. M. E. Flatté, A. A. Kornyshev, and M. Urbakh, *J. Phys. Condens. Matter*, 2008, **20**, 73102.
7. A. G. Volkov, D. W. Deamer, D. L. Tanelian, and V. S. Markin, *Prog. Surf. Sci.*, 1996, **53**, 1–134.
8. E. Smirnov, M. D. Scanlon, D. Momotenko, H. Vrubel, M. a Méndez, P.-F. Brevet, and H. H. Girault, *ACS Nano*, 2014, **8**, 9471–9481.
9. E. Smirnov, P. Peljo, M. D. Scanlon, and H. H. Girault, *ACS Nano*, 2015, **9**, 6565–6575.
10. M. D. Scanlon, P. Peljo, M. A. Méndez, E. Smirnov, and H. H. Girault, *Chem. Sci.*, 2015, **6**, 2705–2720.
11. P. Peljo, E. Smirnov, and H. H. Girault, *J. Electroanal. Chem.*, 2016, **779**, 187–198.
12. L. Isa, F. Lucas, R. Wepf, and E. Reimhult, *Nat. Commun.*, 2011, **2**, 438.